Atmospheric Environment 178 (2018) 214–222

Contents lists available at ScienceDirect

Atmospheric Environment

journal homepage: www.elsevier.com/locate/atmosenv

Mapping nighttime $PM_{2.5}$ from VIIRS DNB using a linear mixed-effect model

D. Fu[a,b], X. Xia[a,b,c,*], M. Duan[a,b], X. Zhang[d], X. Li[e], J. Wang[f], J. Liu[g]

[a] LAGEO, Institute of Atmospheric Physics, Chinese Academy of Sciences, Beijing, 100029, China
[b] College of Earth Sciences, University of Chinese Academy of Sciences, Beijing, 100049, China
[c] Collaborative Innovation Center on Forecast and Evaluation of Meteorological Disasters, Nanjing University of Information Science & Technology, Nanjing 210044, China
[d] School of Atmospheric Sciences, Plateau Atmosphere and Environment Key Laboratory of Sichuan Province, Chengdu University of Information Technology, Chengdu, 610225, China
[e] National Satellite Meteorological Center, China Meteorological Administration, Beijing, 100082, China
[f] Department of Chemical and Biochemical Engineering, Center for Global and Regional Environmental Studies, and Informatics Initiative, The University of Iowa, Iowa City, IA 52241, USA
[g] Beijing Meteorological Bureau, Beijing, 100081, China

A R T I C L E I N F O

Keywords:
VIIRS/DNB
Nighttime $PM_{2.5}$
Mixed effect model

A B S T R A C T

Estimation of particulate matter with aerodynamic diameter less than 2.5 μm ($PM_{2.5}$) from daytime satellite aerosol products is widely reported in the literature; however, remote sensing of nighttime surface $PM_{2.5}$ from space is very limited. $PM_{2.5}$ shows a distinct diurnal cycle and $PM_{2.5}$ concentration at 1:00 local standard time (LST) has a linear correlation coefficient (R) of 0.80 with daily-mean $PM_{2.5}$. Therefore, estimation of nighttime $PM_{2.5}$ is required toward an improved understanding of temporal variation of $PM_{2.5}$ and its effects on air quality. Using data from the Day/Night Band (DNB) of the Visible Infrared Imaging Radiometer Suite (VIIRS) and hourly $PM_{2.5}$ data at 35 stations in Beijing, a mixed-effect model is developed here to estimate nighttime $PM_{2.5}$ from nighttime light radiance measurements based on the assumption that the DNB-$PM_{2.5}$ relationship is constant spatially but varies temporally. Cross-validation showed that the model developed using all stations predict daily $PM_{2.5}$ with mean determination coefficient (R^2) of 0.87 ± 0.12, 0.83 ± 0.10, 0.87 ± 0.09, 0.83 ± 0.10 in spring, summer, autumn and winter. Further analysis showed that the best model performance was achieved in urban stations with average cross-validation R^2 of 0.92. In rural stations, DNB light signal is weak and was likely smeared by lunar illuminance that resulted in relatively poor estimation of $PM_{2.5}$. The fixed and random parameters of the mixed-effect model in urban stations differed from those in suburban stations, which indicated that the assumption of the mixed-effect model should be carefully evaluated when used at a regional scale.

1. Introduction

Much attention has been paid to particulate matter (PM) since it changes the radiative budget of earth-atmosphere system, reduces surface visibility, and influences precipitation. More importantly, surface PM with aerodynamic diameter less than 2.5 μm ($PM_{2.5}$) has adverse effects on human health. Long-term exposure to high $PM_{2.5}$ concentrations may damage cardiovascular and respiratory systems, lead to asthma, lung cancer and increase mortality (Pope and Dockery, 2006).

Measurements of $PM_{2.5}$ concentration with high temporal and spatial resolutions are required for improving our understanding of its effects on environment, climate and human health. Traditional ground observations provide real-time $PM_{2.5}$ measurements with high temporal resolution. Regional networks have been established in developed countries. However, ground observations still have limited spatial coverage over the global land, especially over the developing countries. In contrast, satellite remote sensing is one of the promising methods to estimate surface $PM_{2.5}$ with high spatial resolution at a regional and even global scale, which has been widely suggested more than one decade ago (An et al., 2007; Chu et al., 2003; Fernando et al., 2012; Liu et al., 2009, 2007; Wang and Christopher, 2003). The most popular satellite-derived product for estimating surface $PM_{2.5}$ concentrations is aerosol optical depth (AOD). AOD is indicative of the integrated light extinction of particles in the atmosphere. In early work by Wang and Christopher (2003), the potential of using satellite-based AOD from the Moderate Resolution Imaging Spectroradiometer (MODIS) to derive surface $PM_{2.5}$ concentrations was demonstrated, but the importance of other factors affecting such derivation including mixing layer depth and relative humidity was also recognized. Further studies have attempted to improve the $PM_{2.5}$-AOD relationship through many linear and

* Corresponding author. LAGEO, Institute of Atmospheric Physics, Chinese Academy of Sciences, China.
E-mail address: xxa@mail.iap.ac.cn (X. Xia).

https://doi.org/10.1016/j.atmosenv.2018.02.001
Received 24 August 2017; Received in revised form 29 January 2018; Accepted 1 February 2018
Available online 05 February 2018
1352-2310/

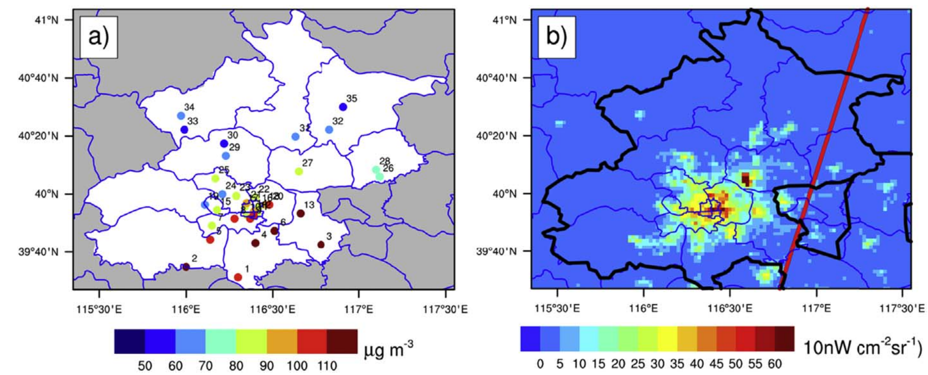

Fig. 1. a) Annual $PM_{2.5}$ mass concentrations at 35 sites (1:00 LST, VIIRS overpass time); b) spatial distribution of annual mean DNB radiance (10 $nWcm^{-2}sr^{-1}$). The red line in panel (b) denotes CALIOP ground track on 07 December 2013. (For interpretation of the references to colour in this figure legend, the reader is referred to the Web version of this article.)

nonlinear statistical models in which additional parameters such as local meteorology and land use information are introduced to develop multiple linear regression model (Gupta and Christopher, 2009a), geographically weighted regression model (Ma et al., 2014; Song et al., 2014), nonlinear model (You et al., 2015), land use regression models (Hoek et al., 2008; Ross et al., 2007), artificial neural networks (Gupta and Christopher, 2009b), optimal estimation algorithm based on transport model (Van Donkelaar et al., 2013), to name just a few. The common feature of these methods is that the $PM_{2.5}$-AOD relationship is developed from short- or long-term simultaneous measurements of $PM_{2.5}$ and AOD as well as other spatiotemporally collocated parameters. Since aerosol properties and their vertical profiles vary day by day, $PM_{2.5}$-AOD relationship should vary temporally, which cannot be completely captured by these linear or nonlinear methods. This is likely one of the reasons why these methods generally predict < 60% of the variability in $PM_{2.5}$ (Hoff and Christopher, 2009).

Lee et al. (2011) introduced a novel mixed-effect model to explain day-specific $PM_{2.5}$-AOD relationship. The coefficient of determination of the model (R^2) can reach 0.92, indicating that this method is promising, especially in those regions with ground-based $PM_{2.5}$ monitoring network. Application of this method in Beijing showed good performance with cross-validations R^2 of 0.75–0.79 (Xie et al., 2015).

AODs applied in previous studies are retrieved from satellite measurements of reflected sunlight. $PM_{2.5}$ concentrations often have a distinct diurnal cycle, which indicates that estimating nighttime $PM_{2.5}$ is absolutely important (Li et al., 2014). Wang et al. (2016) initiated a method to achieve this goal by using a multivariate regression model with nighttime light radiance data from the Day/Night Band (DNB) of the Visible Infrared Imaging Radiometer Suite (VIIRS). Compared to the model considering meteorological variables only (R^2 of 0.25), the model with consideration of DNB data showed better performance (R^2 of 0.45), which suggested that DNB had the potential for monitoring $PM_{2.5}$ concentrations. They further showed that $PM_{2.5}$ mass concentration at VIIRS night-time overpass time (~1:00, local standard time (LST)) better represented daily-mean $PM_{2.5}$ mass concentration than the $PM_{2.5}$ concentration measured during VIIRS or MODIS overpass time during the local noon time. Hence, deriving surface $PM_{2.5}$ from DNB at night is of high value for air quality assessment because daily-mean $PM_{2.5}$ concentration is the parameter widely used by different environmental protection agencies around the world (Wang et al., 2016).

Beijing, the capital of the largest developing country in the world, China, has been suffering heavy air pollution in recent years, especially in winter. For example, a persistent $PM_{2.5}$ pollution event in winter of 2012–2013 was characterized by a maximum hourly $PM_{2.5}$ concentration of 600 $\mu g\,m^{-3}$ (Zheng et al., 2015a). A regional $PM_{2.5}$ network has been established in Beijing and hourly $PM_{2.5}$ concentrations have been available since 2013, which provides opportunities to study seasonality of $PM_{2.5}$ (Zheng et al., 2015b), potential contribution of local emission and long-range transport to heavy $PM_{2.5}$ pollution (Yang et al., 2016).

The objective of this study is to develop a novel method to estimate nighttime $PM_{2.5}$ from space. While this topic has been addressed in previous studies (Wang et al., 2016; McHardy et al., 2015), this paper differs in following ways. **We derived spatial distribution of AOD and thereby mapped surface $PM_{2.5}$ concentration based on VIIRS DNB measurements for the first time in Beijing. Additionally, we adopted a mixed-effect model to establish the relationship between VIIRS DNB derived AOD and $PM_{2.5}$ concentration. Cross-validations showed that the model could predict nighttime hourly $PM_{2.5}$ concentrations with average R^2 of 0.85, indicating DNB's potential in the monitoring of surface $PM_{2.5}$ concentration.** Advantages and disadvantages of this method are discussed in detail.

2. Data and method

2.1. Surface $PM_{2.5}$ mass concentration data

Hourly $PM_{2.5}$ data from 1st December in 2013 to 30th November in 2014 at 35 sites (Fig. 1) are obtained from the website (http://zx.bjmemc.com.cn/). $PM_{2.5}$ concentrations are measured by the Tapered Element Oscillating Microbalance (TEOM). The TEOM's filter is heated to avoid particle-bound water that may result in a slight underestimation of $PM_{2.5}$ mass concentration owing to volatilization of semi-volatile material (Grover et al., 2005). The data are checked for quality according to the environmental protection standard of China. Intercomparison of $PM_{2.5}$ concentrations from the Beijing U.S. diplomatic post and the nearby Ministry of Environmental Protection site indicated a good agreement.

2.2. VIIRS DNB data

The VIIRS, aboard Suomi National Polar-orbiting Partnership (S-NPP), has 22-band channels with a high nominal spatial resolution of 375 m in the five imagery bands (I-bands) and 750 m in the 16 moderate-resolution bands (M-bands). The outstanding feature of VIIRS is that: (a) it is able to detect visible signal in both day and night by its DNB (Polivka et al., 2016), and (b) the spatial resolution of the pixel is increased only by a factor of ~2 from nadir to the edge of the swatch (while in case of MODIS, it is a factor of 8–10) (Polivka et al., 2015). The VIIRS DNB is designed to have a broad spectral coverage (500–900 nm), half maxima of the spectral response function at 700 nm, high spatial resolution of 0.74 × 0.74 km across a 3000-km-wide swath. While the spectral coverage of DNB is wide, DNB is shown to be sensitive to the change of aerosol loading and is not sensitive to the water vapor in urban environment because the spectra of modern city lights does not overlap with water vapor and oxygen absorbing lines (Wang et al., 2016). DNB's amplification gain varies dynamically from three simultaneously collecting stages (groups of detectors) and

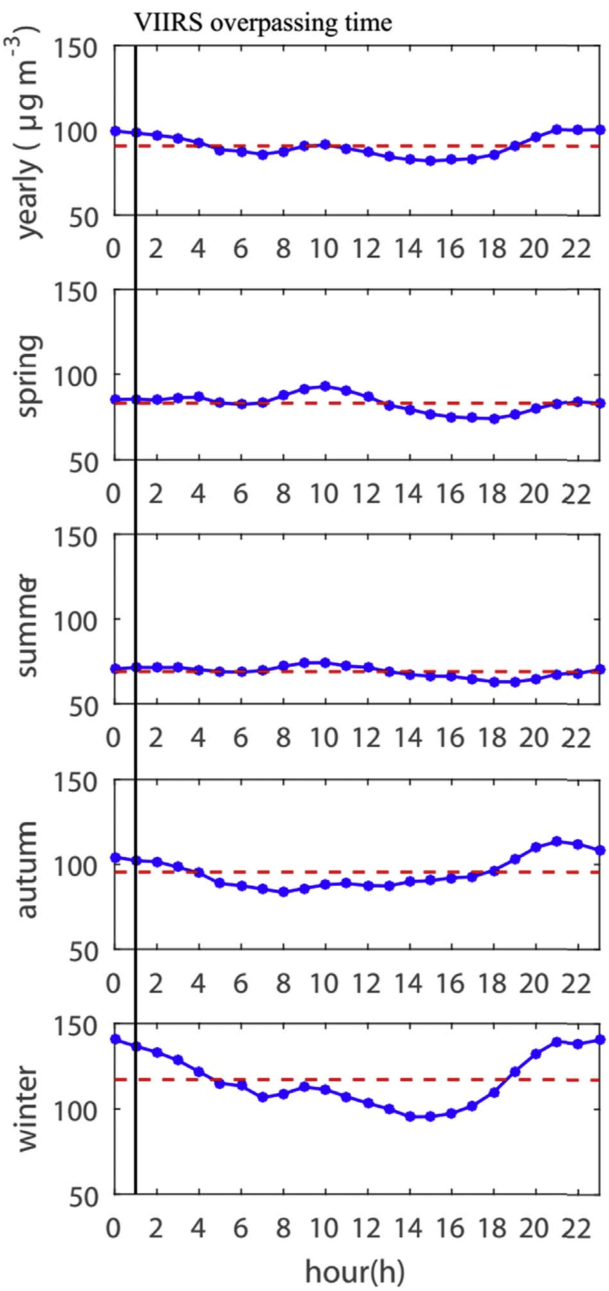

Fig. 2. Diurnal variation (solid line) and daily mean (dot line) of hourly $PM_{2.5}$ concentrations for different seasons. The diurnal variation is the mean of all sites within region and overlaid (in black solid line) is the VIIRS overpass time at night.

these stages enable the DNB to cover the dynamic range of radiances during the daytime, twilight, and nighttime. Compared with its predecessor, the Operational Linescan System (OLS), the DNB has full calibration, improved spatial resolution (0.74 km vs. 2.7 km) and increased radiometric resolutions (14-bit vs. 6-bit) (Lee et al., 2006).

Three datasets of VIIRS were used in this research. The VIIRS Cloud Cover/Layers Height Data Content Summary (VCCLO) was used to filter cloud contamination. The VIIRS/DNB Sensor Data Record-SDR (SVDNB) provided radiance values and quality flag information. The VIIRS/DNB SDR Geolocation Content Summary (GDNBO) provided the corresponding latitude, longitude, solar zenith angle, lunar zenith angle, lunar illumination fraction, and satellite zenith angle data. The data were downloaded from NOAA's Comprehensive Large Array-data Stewardship System (CLASS) (https://www.class.ncdc.noaa.gov/saa/products) (Johnson et al., 2013). A gridded data with 0.01° resolution were produced from the cloud-screened DNB swath data. The mean and standard deviation of the radiances of each 4 × 4 grids were calculated. Hourly $PM_{2.5}$ data close to the overpass time of VIIRS (1:00 LST) were collocated with DNB radiances at each station.

2.3. Model development

A mixed-effect model with random intercepts and slopes for the estimation of $PM_{2.5}$ from AOD is as follows (Lee et al., 2011).

$$PM_{i,j} = (\alpha+u_j) + (\beta+v_j)AOD_{i,j} + s_i + \varepsilon_{i,j} \tag{1}$$

$$(u_j v_j \sim N[(00), \textstyle\sum])$$

where $PM_{i,j}$ represents $PM_{2.5}$ value at site i on day j; α and β represent fixed intercept and slope respectively, which are the conventional linear regression part; u_j and v_j are the random intercept and slope, which explain the day-to-day variations of the AOD-$PM_{2.5}$ relationship influenced by meteorology, pollution transportation, etc. Random effects have prior normal distributions with mean value of 0 and constant variance (Pinheiro and Bates, 2000). $s_i \sim N(0, \sigma_s^2)$ and $\varepsilon_{i,j} \sim N(0, \sigma^2)$ represent the random intercept of site i and the error term at site i on day j. σ_s^2 and σ^2 denote the variances for s_i and $\varepsilon_{i,j}$. Σ is the variance-covariance matrix for the day-specific random effects. s_i accounts for site-specific characteristics, such as topography and pollution emissions.

DNB Radiance (I_{sat}) is related to atmospheric optical depth (τ) as follows if multiple scattering is neglected.

$$I_{sat} = I_a e^{-\tau/\mu} \tag{2}$$

where μ is the cosine of the satellite zenith angle and I_a is the upward visible radiation from the surface. I_a can be generally estimated by I_{sat} from a moonless night with low aerosol loading during certain period. Assuming that I_a at a given location is constant in time and taking the spatial derivative of Equation (2), τ can be estimated using the following equation.

$$\tau = -\mu \ln\left(\frac{\Delta Isat}{C\Delta Ia}\right) \tag{3}$$

Where ΔIsat and ΔIa are pixel-to-pixel differences in satellite-observed radiance and upwelling radiance from surface artificial light source (McHardy et al., 2015). Taking the same strategy as McHardy et al. (2015), ΔIsat is represented by the standard deviations of satellite-observed radiances within one grid (4–8 pixels of DNB). Assuming that city light changes little within three months, the largest ΔIsat with the lunar illumination fraction < 50% is used to represent ΔIa for each season. The rationale behind it is that the largest variance in city should be observed during the night with the lowest aerosol loading and least lunar illumination, which can be used to represent the variation of upwelling radiance from surface artificial light source with little atmospheric contamination. Introduction of parameter C is to correct the dependence of DNB radiance in the absence of cloud, moon and aerosol on μ in some cases, as suggested by Johnson et al. (2013). The correction has been performed only if the coefficient of correlation between μ and DNB radiance in the absence of cloud, moon and aerosol is > 0.6, otherwise, no correction has been performed.

τ derived from equation (3) is mainly attributable to aerosol, although Rayleigh scattering exert somewhat effects (Wang et al., 2016). We can obtain a new model to estimate $PM_{2.5}$ from DNB radiance directly according to Equations (1) and (3) based on collocated $PM_{2.5}$-DNB data points.

$$PM_{i,j} = (\alpha+u_j) + (\beta+v_j)\left(-\mu_{i,j}\ln\left(\frac{\Delta I_{i,j}}{C_i \Delta Ia_{i,j}}\right)\right) + s_i + \varepsilon_{i,j} \tag{5}$$

To evaluate the performance of the model, a cross validation (CV) was implemented (Wilks, 2011). Suppose that we have collocated $PM_{2.5}$

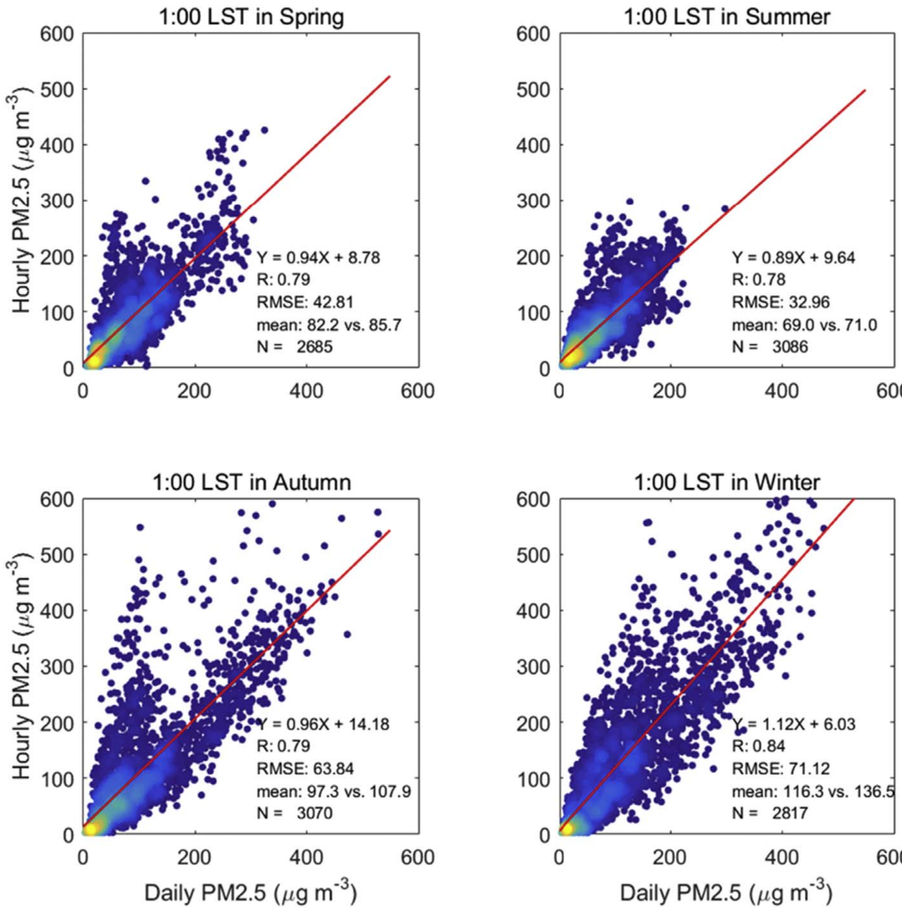

Fig. 3. Inter-comparison between daily-mean (x-axis) $PM_{2.5}$ concentration and the corresponding $PM_{2.5}$ concentration measured at 1:00 LST for four seasons.

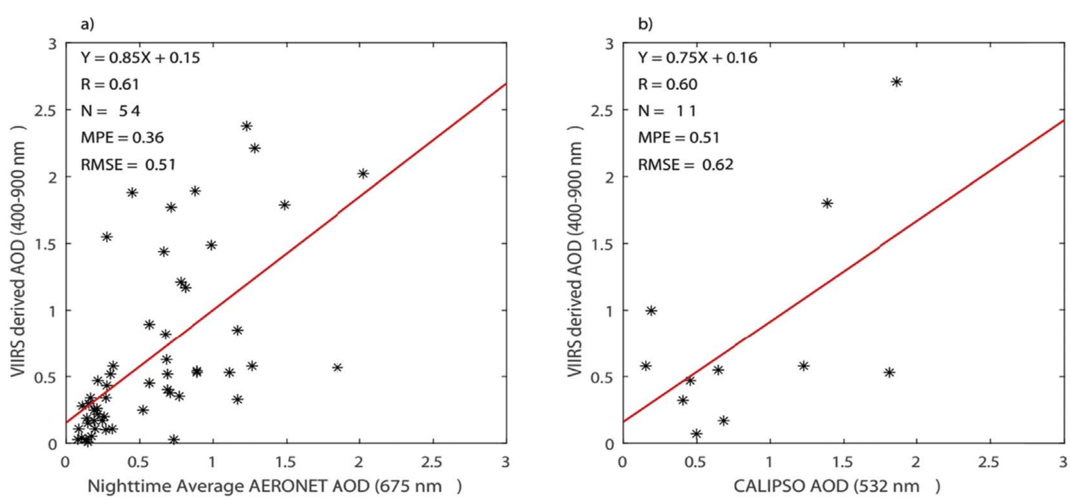

Fig. 4. a) Comparison between the nighttime averaged AERONET AOD and VIIRS derived AOD at Beijing site during 2013–2014; b) Comparison between CALIPSO AOD and VIIRS derived AOD.

and DNB data at N stations, only data at N-1 stations are used to train the model while the data at the remaining station are used to evaluate the model each time. This leave-one-out process was repeated for each of the N sites, which follows the same procedure as in past studies for cross-validation (Wang et al., 2016; Xie et al., 2015). R^2, mean prediction error (MPE), and root-mean-square-error (RMSE) are used to evaluate the performance of the model.

2.4. AOD validation

Two AOD datasets were adopted to validate the values derived from the VIIRS DNB. From the AErosol RObotic NETwork (AERONET), we chose the Level 2.0 data at Beijing site (116.38°, 39.98°) corresponding to the study period. To be comparable with the AOD values of VIIRS DNB, the nighttime τ values were calculated by taking the average of before- and after-overpass AERONET data. The AERONET observations adjacent the VIIRS nighttime overpass were not used if their time difference was more than 24 h (Johnson et al., 2013).

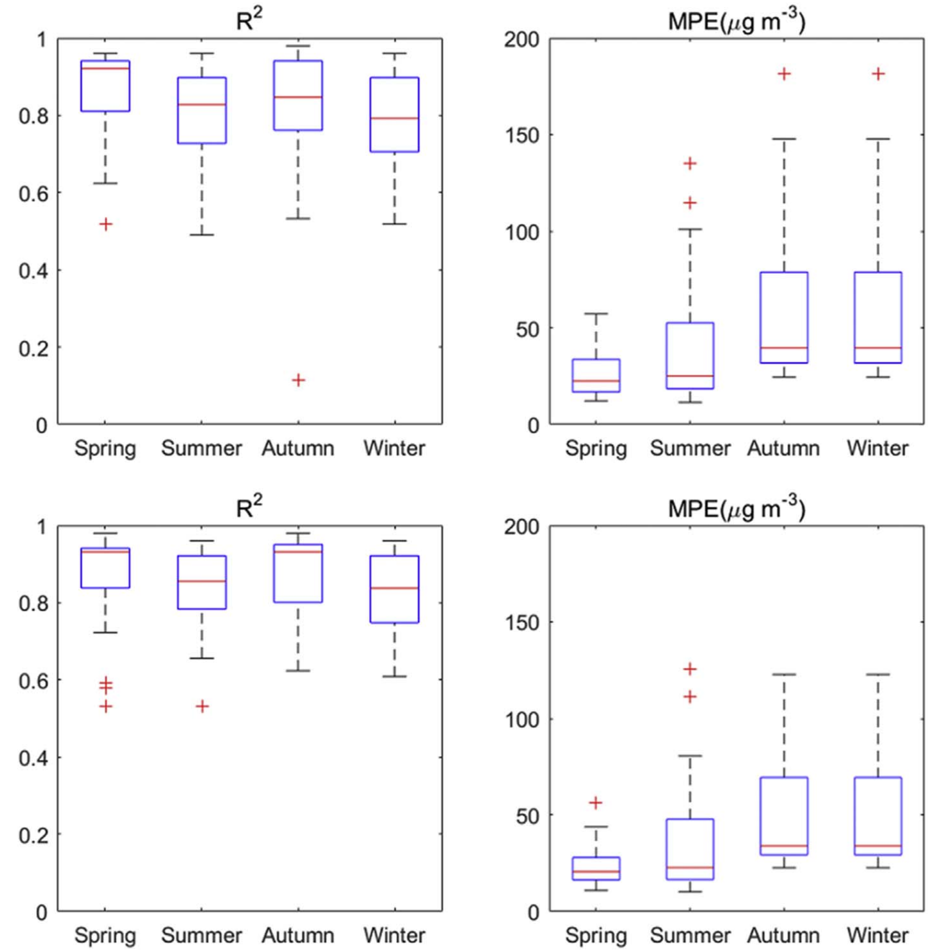

Fig. 5. Box plots of R^2 (left) and MPE ($\mu g\ m^{-3}$) (right) derived from the mixed-effect model with all 35 sites (upper) and 28 sites (lower).

Apart from validation from ground measurements, Cloud-Aerosol LIdar with Orthogonal Polarization (CALIOP) nighttime τ data are also used. The equator crossing time of the CALIOP instrument aboard Cloud and Aerosol Lidar and Infrared Pathfinder Spaceborne Observations (CALIPSO) is about 13:30 and 01:30 local time. CALIOP acquires vertical profiles of elastic backscatter at two wavelengths (532 and 1064 nm) and provides new insight into the vertical distribution of clouds and aerosols over the globe (Winker et al., 2010). In this study the version 4.10 level 2, 5 km aerosol layer product is used, which provides the layer AOD and the column AOD at wavelengths of 0.532 μm and 1.064 μm. The column AOD in the CALIPSO data products is computed by integrating all of the aerosol extinction coefficients with altitude. For comparisons, we consider only cloud-free and quality-controlled aerosol products. That is, we require CALIPSO Extinction QC 532 = 0, indicating that initial lidar ratio unchanged during solution process. We also require cloud-aerosol discrimination (CAD) score to be less than 0 and greater than −100, since negative value signifies aerosol and the absolute value of CAD indicates a confidence level.

Different from the AERONET Beijing's validation, there is a lack of collocated CALIOP and VIIRS data pairs over Beijing area and the matchups are usually located in rural area with no sufficient artificial light sources (Fig. 1b). To obtain more data for the comparison, we expand the comparison area to the entire rectangular area. In temporal collocation, we choose CALIPSO closest-approaches that are within 2-h of a VIIRS measurement.

3. Results

3.1. Diurnal and seasonal variations of $PM_{2.5}$ concentration

Annual mean $PM_{2.5}$ measured at 35 sites is 90.8 $\mu g\ m^{-3}$. Seasonal averaged $PM_{2.5}$ concentrations for spring, summer, autumn and winter are 82.2 ± 5.1 $\mu g\ m^{-3}$, 69.0 ± 3.1 $\mu g\ m^{-3}$, 97.3 ± 9.0 $\mu g\ m^{-3}$ and 116.3 ± 15.2 $\mu g\ m^{-3}$, respectively. The seasonal variations can be attributable to seasonal variations of emission and meteorological conditions. For example, heavy pollution in winter is likely associated with coal burning for heating and shallow boundary layer depth (Li et al., 2014). Spatially, there is a gradient of surface $PM_{2.5}$ from south to north due to specific topography and population distribution in Beijing (Fig. 1a). Northwest of Beijing is surrounded by mountains, while south sites are more influenced by local anthropogenic emissions of aerosols and long-range transport of aerosols from south of Beijing.

Diurnal characteristics of $PM_{2.5}$ concentrations vary with seasons (Fig. 2). **The variations in spring and winter appear** a flat "W" shape with relative lower value at 06:00–07:00 LST and 15:00–17:00 LST. There is an increasing trend of concentrations during 7:00–10:00 LST that is likely associated with enhanced anthropogenic activities during rush hour. The decreasing trend at 10:00–15:00 LST **in winter** can be explained as follows. The boundary layer usually begins to form after sunrise and the depth grows gradually into the afternoon. The increase of boundary layer depth provides a larger volume for the dilution of pollutants, resulting in a reduction of $PM_{2.5}$ concentrations in the afternoon. Although emission and removal of particles by deposition decrease during night, $PM_{2.5}$ concentration increases as the boundary layer depth decreases (Miao et al., 2009). **Different from that in**

Table 1
Site information of 35 monitoring sites in Beijing.

Site	Lon (°)	Lat (°)	N	Radiance	$PM_{2.5}$ ± STD ($\mu g\, m^{-3}$)	R_m
MYSK	116.91	40.50	203	1.4 ± 17.8	53.5 ± 57.6	0.50
BDL	115.99	40.37	286	2.0 ± 15.9	50.4 ± 51.8	0.59
DL	116.22	40.29	258	2.4 ± 14.8	54.6 ± 66.8	0.51
DGC	117.12	40.10	276	2.8 ± 16.0	70.9 ± 66.0	0.53
ZWY	116.21	40.01	247	3.6 ± 19.7	68.65 ± 73.0	0.37
LLH	116.00	39.58	233	3.6 ± 15.4	133.5 ± 110.2	0.57
YF	116.30	39.52	244	4.3 ± 7.0	104.4 ± 81.6	0.54
YLD	116.78	39.71	262	6.4 ± 4.1	121.5 ± 111.8	0.37
YG	116.15	39.82	272	9.4 ± 2.9	85.2 ± 81.3	0.41
BBXQ	116.17	40.09	274	9.7 ± 12.8	81.8 ± 74.0	0.34
HR	116.63	40.33	256	13.5 ± 3.9	63.1 ± 63.1	0.30
YQ	115.97	40.45	291	14.1 ± 11.0	69.5 ± 63.3	0.19
DX	116.40	39.72	276	17.1 ± 7.6	114.9 ± 104.3	0.20
PG	117.10	40.14	276	18.7 ± 7.5	76.2 ± 74.9	0.28
FS	116.14	39.74	269	20.8 ± 14.5	100.5 ± 89.4	0.22
WL	116.29	39.99	250	22.9 ± 12.3	88.4 ± 79.3	0.21
SY	116.65	40.13	281	23.2 ± 9.1	85.4 ± 77.0	0.19
MY	116.83	40.37	276	25.6 ± 17.8	68.5 ± 75.5	0.15
MTG	116.11	39.94	261	28.2 ± 11.0	67.6 ± 69.2	0.21
YDMN	116.39	39.88	269	29.3 ± 7.7	101.4 ± 83.8	0.19
XZMB	116.35	39.95	260	30.4 ± 6.6	90.7 ± 82.1	0.17
GC	116.18	39.91	274	30.9 ± 11.4	81.6 ± 72.0	0.17
DSH	116.48	39.94	266	33.0 ± 7.2	103.9 ± 99.9	0.18
TZ	116.66	39.89	253	34.1 ± 2.4	124.8 ± 115.9	0.20
CP	116.23	40.22	267	34.2 ± 2.1	66.3 ± 70.2	0.06
YZ	116.51	39.79	268	35.1 ± 1.9	112.9 ± 96.7	0.16
NSH	116.37	39.86	252	36.4 ± 2.3	104.5 ± 89.6	0.11
FTHY	116.28	39.86	271	37.8 ± 3.4	101.1 ± 92.9	0.14
NZG	116.46	39.94	275	39.9 ± 3.1	93.6 ± 90.5	0.16
GY	116.34	39.93	269	40.0 ± 2.7	86.5 ± 75.0	0.16
WSXG	116.35	39.88	267	40.2 ± 16.1	88.5 ± 80.2	0.10
DS	116.42	39.93	278	43.9 ± 8.9	87.9 ± 80.2	0.18
TT	116.41	39.89	272	44.8 ± 9.9	84.7 ± 74.7	0.16
QM	116.39	39.9	269	45.2 ± 12.9	99.0 ± 87.6	0.16
ATZX	116.40	39.98	271	48.9 ± 10.3	88.4 ± 77.8	0.09

(Noted: N represents day number with collocated $PM_{2.5}$ and DNB data. $PM_{2.5}$ ± STD represents mean and standard deviation of $PM_{2.5}$ concentrations during the overpassing time of VIIRS. R_m is the linear correlation coefficient between DNB radiance and the lunar illumination fraction. The unit of radiance is $nWcm^{-2}sr^{-1}$).

Table 2
Model performance of cross validation based on result from all 35 sites and 28 sites with $R_m > 0.4$, respectively.

	Slope[a]	Intercept[b] (P < 0.00001)	R^2	MPE[c] ($\mu g\, m^{-3}$)	RMSE[d] ($\mu g\, m^{-3}$)
35 sites (all sites)					
Spring	76.63 ± 7.79	1.60 ± 1.74	0.86	46.1	25.5
Summer	62.24 ± 5.38	2.61 ± 1.10	0.80	41.1	12.4
Autumn	89.80 ± 10.51	4.66 ± 2.89	0.83	57.9	41.2
Winter	122.58 ± 12.66	2.57 ± 2.39	0.80	56.2	52.3
28 sites (sites with R_m < 0.4 only)					
Spring	75.69 ± 8.12	5.23 ± 2.61	0.87	34.2	23.7
Summer	62.91 ± 5.48	4.15 ± 1.44	0.83	35.5	20.7
Autumn	90.77 ± 11.00	4.14 ± 2.17	0.87	48.1	36.6
Winter	127.58 ± 12.88	−0.10 ± 2.60	0.83	45.7	48.4

(Slope[a] and Intercept[b] are the fixed terms of regression slope and regression intercept. MPE[c] and RMSE[d] are the absolute differences and the root mean squared differences between predicted and measured $PM_{2.5}$ concentrations.).

autumn and winter, a flat diurnal variation was observed in spring, which was likely a reflection of a faint variation of the boundary layer depth. The second peak in spring was corresponded to rush-hour or cooking time. The smallest diurnal fluctuation was observed in summer, which was likely associated with strong dispersion and deposition.

In diurnal variation patterns, $PM_{2.5}$ concentrations during VIIRS overpass time at night (1:00 LST) are representative of daily-mean $PM_{2.5}$ with bias percentages of 4.1%, 3.0%, 10.9% and 17.4% for four seasons, respectively. Besides, it should be noted that $PM_{2.5}$ concentrations in mid-morning (10:00 LST, MODIS/Terra overpass time) and early-afternoon (13:00 LST, MODIS/Aqua daytime overpass) are also representative of daily mean of $PM_{2.5}$ (Wang et al., 2016; Wang and Christopher, 2003). Further analysis (Fig. 3) shows that $PM_{2.5}$ at 1:00 LST is correlated with corresponding daily-mean $PM_{2.5}$ (R = 0.80) with mean RMSE of 52.7 $\mu g\, m^{-3}$, which indicates the potential of $PM_{2.5}$ derived from VIIRS DNB at night for assessing daily-mean air quality.

3.2. AOD validation

Fig. 4a shows VIIRS-retrieved AOD against the corresponding straddling daytime-averaged AERONET AOD for Beijing site **(R = 0.61).** As daytime AOD may not be the ideal dataset for validation, Fig. 4b presents the results of VIIRS-derived AOD against CALIPSO AOD (R = 0.60, MPE of 0.51). The limited sample number (N = 11) is due to insufficient data pairs of collocated CALIOP and VIIRS. Though the performances of both validation methods are some similar, it should be noted that the areas for comparison are different. The former is a comparison over one site and the main uncertainty may come from the averaged AERONET AOD representing nighttime τ. The latter is a comparison over different grid cells and the uncertainty is mainly due to no sufficient artificial lights for VIIRS retrieving. Furthermore, AOD from CALIOP also have uncertainties of 0.1 (Kittaka et al., 2011), and can be up to 0.3 in heavy polluted cases (Ma et al., 2013).

3.3. Establishment of the mixed-effect model

Table 2 presents cross validation results from 35 sites and 28 sites (7 sites are eliminated since values of $R_m < 0.4$). The fixed slope shows a clear seasonal dependence. More specific, the slope in winter is nearly twice larger than that in summer, indicating that a fixed linear or nonlinear model cannot capture the real complicated $PM_{2.5}$-AOD relationships, especially based on long-term collocated data. Seasonal R^2 ranges from 0.80 to 0.86. **However, a significant spatial variation of R^2 is observed and the site-specific R^2 ranges from 0.11 to 0.98 (Fig. 5).** Abnormally low R^2 values are derived in sites with weak upwelling radiance, for example, at BDL, a site close to the Great Wall. The signal of DNB radiance at this site is probably affected by lunar illumination, which is supported by the fact that R_m exceeds 0.4. This indicates that caution should be taken to use DNB to estimate $PM_{2.5}$ in rural areas where artificial light is limited. The model is established after 7 sites (MYSK, BDL, DGC, DL, LLH, YF and YG where $R_m > 0.4$ in Table 1) are excluded. The obvious improvement of the model performance is clearly shown in Table 2 and Fig. 5. The overall MPE and RMSE are 40.9 $\mu g\, m^{-3}$ and 32.4 $\mu g\, m^{-3}$, respectively, 23.1% and 9.5% lower than the values from the model established using data at all 35 sites. Annual average R^2 is 0.85 and the seasonal average R^2 of spring, summer, autumn and winter are 0.87 ± 0.12, 0.83 ± 0.10, 0.87 ± 0.09, 0.83 ± 0.10, respectively. **Compared with the daytime mixed-effect model in Beijing (R^2 of 0.75 − 0.79) (Xie et al., 2015), our nighttime model performs better. This is likely because a well-mixed aerosols within a shallow nocturnal boundary layer during midnight is favorable for a stable AOD-$PM_{2.5}$ relationship. This is also likely due to more collocated DNB and $PM_{2.5}$ data points than those from daytime AOD and $PM_{2.5}$.**

The model performance after 7 stations are excluded in the model establishment still shows a clear spatial dependence (Fig. 6). Urban area within black rectangular box in Fig. 6 (116.15°E-116.50°E, 39.80°N-40.00°N) is characterized by higher R^2 of 0.91 ± 0.04 than that in rural area (0.78 ± 0.10).

To investigate the site location's effects on the results, analysis is then conducted separately with sites in urban area (14 sites) and rural area (14 sites). Compared with the mixed-effect model with 28 sites, R^2

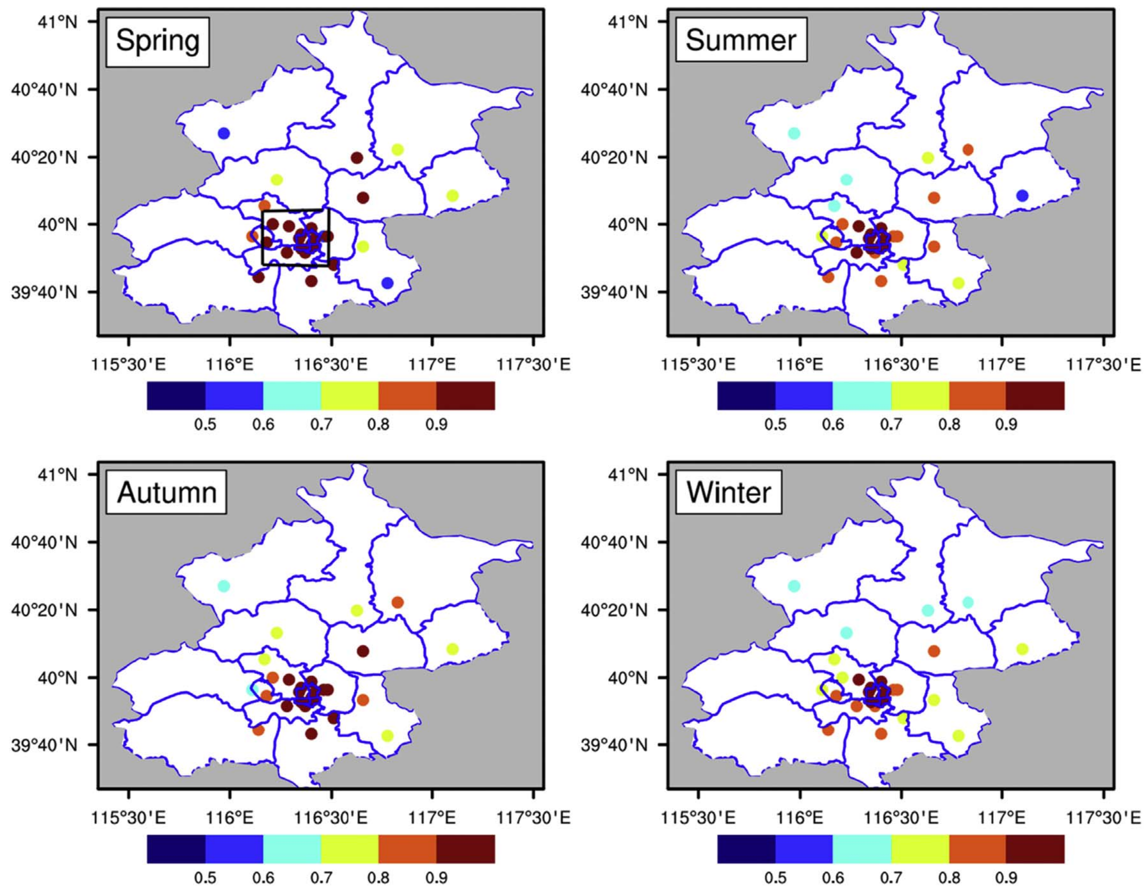

Fig. 6. Spatial variation of R^2 from the mixed-effect model based on data in 28 sites. Rectangular box in Figure indicates urban area.

Table 3
The fixed terms of the mixed-effect models and their performance over 14 urban sites and 14 rural sites, respectively.

Model Type	Slope[a]	Intercept[b] (P < 0.00001)	R^2	MPE[c] ($\mu g\,m^{-3}$)	RMSE[d] ($\mu g\,m^{-3}$)
14 sites in urban area					
Spring	82.74 ± 8.52	−2.12 ± 3.69	0.92	21.2	18.6
Summer	69.39 ± 5.84	3.02 ± 1.96	0.92	15.3	14.5
Autumn	99.01 ± 12.72	1.06 ± 2.47	0.94	24.2	25.7
Winter	120.60 ± 12.13	4.24 ± 3.14	0.92	23.4	32.5
14 sites in rural area					
Spring	68.58 ± 8.04	7.59 ± 2.55	0.84	43.2	26.9
Summer	56.33 ± 5.92	4.63 ± 1.79	0.75	52.5	25.7
Autumn	81.69 ± 11.92	7.71 ± 3.70	0.77	69.2	48.8
Winter	124.58 ± 14.71	2.28 ± 3.58	0.73	73.7	64.9

increases and MPE, RMSE decrease in urban area (R^2 of 0.92–0.94, RMSE of 15.3–24.3 $\mu g\,m^{-3}$, MPE of 14.5–32.5 $\mu g\,m^{-3}$) (Table 3). While the performance of rural sites is relatively poor. The averaged R^2 over four seasons is 0.77 ± 0.10, which is even lower than result obtained from 28 sites (0.85). Worse performance in rural area is possibly due to low DNB signal/noise ratio, a large spatial variation of AOD- $PM_{2.5}$ relationship and **low sample density. 14 sites in rectangular box are almost located in area with strong artificial lights (Fig. 1) and close to each other in space. Hence, the model constructed with these sites will have better performance.**

3.4. Predicted surface $PM_{2.5}$

Mapping surface $PM_{2.5}$ concentrations with valid DNB data was carried out at pixels with $R_m < 0.4$. The site term was replaced by each grid's position based on following reasons. First, site information was not available for each 0.04° resolution grid. Second, higher cross validation R^2 in urban area indicated that the model could be used to predict $PM_{2.5}$ in grids without ground-site measurements. Taking seasonal variation into consideration, we calculated seasonal $PM_{2.5}$ concentrations (Fig. 7). Averaged satellite-derived $PM_{2.5}$ concentrations were 85.5 $\mu g\,m^{-3}$, 71.5 $\mu g\,m^{-3}$, 99.7 $\mu g\,m^{-3}$ and 125.5 $\mu g\,m^{-3}$ for spring, summer, autumn and winter, respectively, which shared the same seasonal properties with site-observed $PM_{2.5}$ concentrations. With fine resolution of $PM_{2.5}$ concentration map, we could see a fine spatial variation of $PM_{2.5}$.

4. Discussion and conclusions

Pronounced diurnal variation of $PM_{2.5}$ concentrations in Beijing is found and nighttime shows some different features against daytime. In addition, $PM_{2.5}$ concentration derived from VIIRS DNB at night, similar with $PM_{2.5}$ derived from MODIS, can be applied to assess daily-mean $PM_{2.5}$ with a R of 0.80. It is therefore worthwhile to retrieve nighttime $PM_{2.5}$ concentrations, which would undoubtedly improve our understanding of diurnal variation of $PM_{2.5}$. This study developed a mixed-effect model to estimate nighttime $PM_{2.5}$ concentrations from VIIRS DNB measurements of artificial light radiance, which was approved to be a promising method to estimate nocturnal $PM_{2.5}$ from space. The VIIRS-derived AODs were also compared with CALIPSO AODs. Cross-validation showed that the mixed-effect model could predict hourly $PM_{2.5}$ (1:00 LST) with R^2 exceeding 0.8. Further analysis showed that the best model performance was achieved in urban stations with R^2 of 0.92. Gridded $PM_{2.5}$ with spatial resolution of 0.04° was produced in Beijing.

One of important advantages of using VIIRS DNB in the estimation

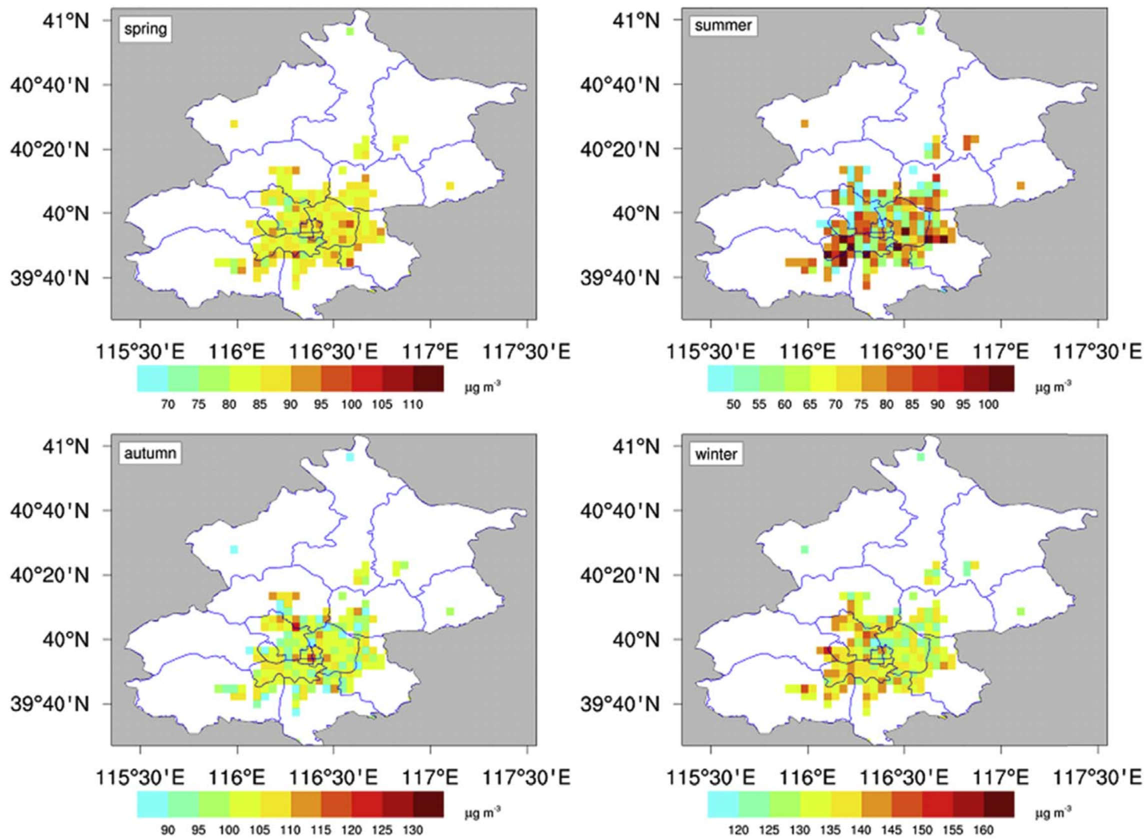

Fig. 7. Mean $PM_{2.5}$ concentrations ($\mu g\ m^{-3}$) derived from VIIRS/DNB in Beijing (grids with $R_m > 0.4$ are eliminated).

of $PM_{2.5}$ was that it could provide more valid estimations than MODIS. The collocated DNB-$PM_{2.5}$ data points during the studied period were 3.0, 1.3, 1.8 and 3.7 times larger than MODIS/AOD-$PM_{2.5}$ points from spring to winter. Fewer MODIS AOD retrievals in winter were likely due to misclassification of heavy aerosol pollution to cloud and occasional snow events.

Limitations of this method should also be kept in mind. First, DNB nighttime radiance measurements are associated with not only surface light emissions but also other factors, for example, lunar illuminance. The model can only be applied in areas with considerable surface light emissions, which limits the spatial coverage of the method. Second, multiple scattering of artificial light needs further study that requires comprehensive radiative transfer model simulations.

Acknowledgements

This work is supported by the National Science Foundation of China (41475138, 41675033, 41175028, 91644217) and the national key research and development program of China (2016YFC0200403).

References

An, X., Zhu, T., Li, C., Wang, Y., 2007. A modeling analysis of a heavy air pollution episode occurred in Beijing. Atmos. Chem. Phys. 7, 3103–3114. https://doi.org/10.5194/acpd-6-8215-2006.

Chu, D. a., Kaufman, Y.J., Zibordi, G., Chern, J.,D., Mao, J., Li, C., Holben, B.N., 2003. Global monitoring of air pollution over land from the earth observing system-terra moderate resolution imaging spectroradiometer (MODIS). J. Geophys. Res. 108, 1–18. https://doi.org/10.1029/2002JD003179.

Fernando, H.J.S., Mammarella, M.C., Grandoni, G., Fedele, P., Di Marco, R., Dimitrova, R., Hyde, P., 2012. Forecasting PM10 in metropolitan areas: efficacy of neural networks. Environ. Pollut. 163, 62–67. https://doi.org/10.1016/j.envpol.2011.12.018.

Grover, B.D., Kleinman, M., Eatough, N.L., Eatough, D.J., Hopke, P.K., Long, R.W., Wilson, W.E., Meyer, M.B., Ambs, J.L., 2005. Measurement of total $PM_{2.5}$ mass (nonvolatile plus semivolatile) with the Filter Dynamic Measurement System tapered element oscillating microbalance monitor. J. Geophys. Res. Atmos. 110, 1–9. https://doi.org/10.1029/2004JD004995.

Gupta, P., Christopher, S.A., 2009a. Particulate matter air quality assessment using integrated surface, satellite, and meteorological products: multiple regression approach. J. Geophys. Res. Atmos. 114, 1–13. https://doi.org/10.1029/2008JD011496.

Gupta, P., Christopher, S.A., 2009b. Particulate matter air quality assessment using integrated surface, satellite, and meteorological products: 2. A neural network approach. J. Geophys. Res. Atmos. 114, 1–14. https://doi.org/10.1029/2008JD011497.

Hoek, G., Beelen, R., de Hoogh, K., Vienneau, D., Gulliver, J., Fischer, P., Briggs, D., 2008. A review of land-use regression models to assess spatial variation of outdoor air pollution. Atmos. Environ. https://doi.org/10.1016/j.atmosenv.2008.05.057.

Hoff, R.M., Christopher, S.A., 2009. Remote sensing of particulate pollution from space: have we reached the promised land? J. Air Waste Manage. Assoc 59, 645–675. https://doi.org/10.3155/1047-3289.59.6.645.

Johnson, R.S., Zhang, J., Hyer, E.J., Miller, S.D., Reid, J.S., 2013. Preliminary investigations toward nighttime aerosol optical depth retrievals from the VIIRS Day/Night Band. Atmos. Meas. Tech 6, 1245–1255. https://doi.org/10.5194/amt-6-1245-2013.

Kittaka, C., Winker, D.M., Vaughan, M.A., Omar, A., Remer, L.A., 2011. Intercomparison of column aerosol optical depths from CALIPSO and MODIS-Aqua. Atmos. Meas. Tech 4, 131–141. https://doi.org/10.5194/amt-4-131-2011.

Lee, H.J., Liu, Y., Coull, B.A., Schwartz, J., Koutrakis, P., 2011. A novel calibration approach of MODIS AOD data to predict $PM_{2.5}$ concentrations. Atmos. Chem. Phys. 11, 7991–8002. https://doi.org/10.5194/acp-11-7991-2011.

Lee, T.E., Miller, S.D., Turk, F.J., Schueler, C., Julian, R., Deyo, S., Dills, P., Wang, S., 2006. The NPOESS VIIRS day/night visible sensor. Bull. Am. Meteorol. Soc. 87, 191–199. https://doi.org/10.1175/BAMS-87-2-191.

Li, R., Li, Z., Gao, W., Ding, W., Xu, Q., Song, X., 2014. Diurnal, seasonal, and spatial variation of $PM_{2.5}$ in Beijing. Sci. Bull. 60, 387–395. https://doi.org/10.1007/s11434-014-0607-9.

Liu, Y., Franklin, M., Kahn, R., Koutrakis, P., 2007. Using aerosol optical thickness to predict ground-level $PM_{2.5}$ concentrations in the St. Louis area: a comparison between MISR and MODIS. Remote Sens. Environ. 107, 33–44. https://doi.org/10.1016/j.rse.2006.05.022.

Liu, Y., Paciorek, C.J., Koutrakis, P., 2009. Estimating regional spatial and temporal variability of $PM_{2.5}$ concentrations using satellite data, meteorology, and land use information. Environ. Health Perspect. 117, 886–892. https://doi.org/10.1289/ehp.0800123.

Ma, X., Bartlett, K., Harmon, K., Yu, F., 2013. Comparison of AOD between CALIPSO and MODIS: significant differences over major dust and biomass burning regions. Atmos. Meas. Tech 6, 2391–2401. https://doi.org/10.5194/amt-6-2391-2013.

Ma, Z., Hu, X., Huang, L., Bi, J., Liu, Y., 2014. Estimating ground-level $PM_{2.5}$ in China using satellite remote sensing. Environ. Sci. Technol. 48, 7436–7444. https://doi.org/10.1021/es5009399.

McHardy, T.M., Zhang, J., Reid, J.S., Miller, S.D., Hyer, E.J., Kuehn, R.E., 2015. An improved method for retrieving nighttime aerosol optical thickness from the VIIRS Day/Night Band. Atmos. Meas. Tech 8, 4773–4783. https://doi.org/10.5194/amt-8-4773-2015.

Miao, S., Chen, F., LeMone, M.A., Tewari, M., Li, Q., Wang, Y., 2009. An observational and modeling study of characteristics of urban heat island and boundary layer structures in Beijing. J. Appl. Meteorol. Climatol 48, 484–501. https://doi.org/10.1175/2008JAMC1909.1.

Pinheiro, J.C., Bates, D.M.C.N.-J. or A.B.R.R.Q. 73. S.P. 2000 J. or A.B.R.R.-S.O.Q. 73. S.P. 2000, 2000. Mixed-effects models in S and S-PLUS. Springer. https://doi.org/10.1016/j.agsy.2005.11.004.

Polivka, T.N., Hyer, E.J., Wang, J., Peterson, D.A., 2015. First global analysis of saturation artifacts in the VIIRS infrared channels and the effects of sample aggregation. IEEE Geosci. Remote Sens. Lett. 12, 1262–1266. https://doi.org/10.1109/LGRS.2015.2392098.

Polivka, T.N., Wang, J., Ellison, L.T., Hyer, E.J., Ichoku, C.M., 2016. Improving nocturnal fire detection with the VIIRS day–night band. IEEE Trans. Geosci. Rem. Sens. 54, 5503–5519. https://doi.org/10.1109/TGRS.2016.2566665.

Pope, C.A., Dockery, D.W., 2006. Health effects of fine particulate air pollution: lines that connect. J. Air Waste Manage. Assoc 56, 709–742. https://doi.org/10.1080/10473289.2006.10464485.

Ross, Z., Jerrett, M., Ito, K., Tempalski, B., Thurston, G.D., 2007. A land use regression for predicting fine particulate matter concentrations in the New York City region. Atmos. Environ. 41, 2255–2269. https://doi.org/10.1016/j.atmosenv.2006.11.012.

Song, W., Jia, H., Huang, J., Zhang, Y., 2014. A satellite-based geographically weighted regression model for regional $PM_{2.5}$ estimation over the Pearl River Delta region in China. Remote Sens. Environ. 154, 1–7. https://doi.org/10.1016/j.rse.2014.08.008.

Van Donkelaar, A., Martin, R.V., Spurr, R.J.D., Drury, E., Remer, L.A., Levy, R.C., Wang, J., 2013. Optimal estimation for global ground-level fine particulate matter concentrations. J. Geophys. Res. Atmos. 118, 5621–5636. https://doi.org/10.1002/jgrd.50479.

Wang, J., Aegerter, C., Xu, X., Szykman, J.J., 2016. Potential application of VIIRS Day/Night Band for monitoring nighttime surface $PM_{2.5}$ air quality from space. Atmos. Environ. 124, 55–63. https://doi.org/10.1016/j.atmosenv.2015.11.013.

Wang, J., Christopher, S., 2003. Intercomparison between satellite-derived aerosol optical thickness and $PM_{2.5}$ mass: implications for air quality studies. Geophys. Res. Lett. 30 (2095). https://doi.org/10.1029/2003GL018174.

Wilks, D.S., 2011. Statistical methods in the atmospheric sciences. Int. Geophys. Ser. https://doi.org/10.1198/jasa.2007.s163.

Winker, D.M., Pelon, J., Coakley, J.A., Ackerman, S.A., Charlson, R.J., Colarco, P.R., Flamant, P., Fu, Q., Hoff, R.M., Kittaka, C., Kubar, T.L., Le Treut, H., McCormick, M.P., Mégie, G., Poole, L., Powell, K., Trepte, K., Vaughan, M.A., Wielicki, B.A., 2010. The CALIPSO mission: a global 3D view of aerosols and clouds. Bull. Am. Meteorol. Soc. 91, 1211–1229. https://doi.org/10.1175/2010BAMS3009.1.

Xie, Y., Wang, Y., Zhang, K., Dong, W., Lv, B., Bai, Y., 2015. Daily estimation of ground-level $PM_{2.5}$ concentrations over Beijing using 3 km resolution MODIS AOD. Environ. Sci. Technol. 49, 12280–12288. https://doi.org/10.1021/acs.est.5b01413.

Yang, W., Wang, G., Bi, C., 2016. Analysis of long-range transport effects on $PM_{2.5}$ during a short severe haze in Beijing, China. Aerosol Air Qual. Res. 17, 1510–1522. https://doi.org/10.4209/aaqr.2016.06.0220.

You, W., Zang, Z., Pan, X., Zhang, L., Chen, D., 2015. Estimating $PM_{2.5}$ in Xi'an, China using aerosol optical depth: a comparison between the MODIS and MISR retrieval models. Sci. Total Environ. 505, 1156–1165. https://doi.org/10.1016/j.scitotenv.2014.11.024.

Zheng, G.J., Duan, F.K., Su, H., Ma, Y.L., Cheng, Y., Zheng, B., Zhang, Q., Huang, T., Kimoto, T., Chang, D., Pöschl, U., Cheng, Y.F., He, K.B., 2015a. Exploring the severe winter haze in Beijing: the impact of synoptic weather, regional transport and heterogeneous reactions. Atmos. Chem. Phys. 15, 2969–2983. https://doi.org/10.5194/acp-15-2969-2015.

Zheng, S., Pozzer, A., Cao, C.X., Lelieveld, J., 2015b. Long-term (2001-2012) concentrations of fine particulate matter ($PM_{2.5}$) and the impact on human health in Beijing, China. Atmos. Chem. Phys. 15, 5715–5725. https://doi.org/10.5194/acp-15-5715-2015.